



Open Archive Toulouse Archive Ouverte

OATAO is an open access repository that collects the work of Toulouse researchers and makes it freely available over the web where possible

This is an author's version published in: <http://oatao.univ-toulouse.fr/22928>

Official URL:

<https://doi.org/10.1016/j.proci.2018.06.047>

To cite this version:

Kaiser, Thomas and Oztarlik, Gorkem and Selle, Laurent and Poinsot, Thierry Impact of symmetry breaking on the Flame Transfer Function of a laminar premixed flame. (2019) Proceedings of the Combustion Institute, 37 (2). 1953-1960. ISSN 1540-7489

Any correspondence concerning this service should be sent to the repository administrator: tech-oatao@listes-diff.inp-toulouse.fr

Impact of symmetry breaking on the Flame Transfer Function of a laminar premixed flame

T.L. Kaiser ^{a,*}, G. Öztarlık ^a, L. Selle ^{a,b}, T. Poinso ^{a,b}

^a *IMFT (Institut de Mécanique des Fluides de Toulouse), 2 Allée Camille Soula, 31400 Toulouse, France*

^b *CERFACS, 42 Avenue Gaspard Coriolis, 31057 Toulouse Cedex 1, France*

Abstract

This work presents a numerical study of the acoustic response of a laminar flame with tunable asymmetry. A V-shaped premixed flame is stabilised in the wake of a cylindrical flame holder that can be rotated. The configuration is symmetric when the flame holder is fixed but increasing its rotation rate breaks the symmetry of the flow. This configuration is submitted to acoustic forcing to measure the effect of rotation of the flame holder on the Flame Transfer Functions. It appears that the asymmetry of the two flame branches changes their respective time delays, resulting in interference in the global unsteady heat release rate fluctuations. Consequently, the Flame Transfer Function exhibits dips and bumps, which are studied via laminar Direct Numerical Simulation. Potential applications for the control of combustion instabilities are discussed.

Keywords: Laminar flame; Symmetry breaking; Interference; Laminar DNS; Rotating cylinder

1. Introduction

Combustion instabilities caused by a coupling of heat release fluctuations and acoustic modes of the combustion chamber are one of the key uncertainties in the development process of gas turbines. Their consequences may range from limiting the operating conditions to the destruction of the combustion chamber.

Combustion instabilities involve various complex physical mechanisms. Therefore, canonical test cases are often used to isolate certain phenom-

ena. In this context, several configurations involving laminar flames in various shapes have been studied in the past. Besides V-flames and conical flames [1,2], the case of a flame anchoring in the wake of a bluff body in laminar cross flow, has been studied using numerical and analytical approaches. Using laminar Direct Numerical Simulations (DNS) validated by experiments, Brebion et al. [3] investigated the influence of the cylindrical flame holder's temperature on the flame anchoring mechanism. In their follow up study, Mejia et al. [4] investigated the influence of the cylinder's temperature on the Flame Transfer Function (FTF). The effect of rotation of the cylinder on the flame anchoring mechanism was explained by Xavier et al. [5] and Mejia et al. [6]. Their results

* Corresponding author.

E-mail address: tkaiser@imft.fr (T.L. Kaiser).

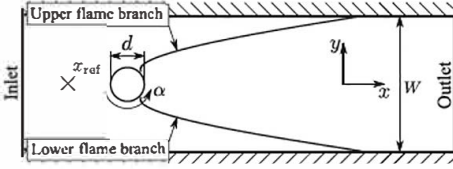


Fig. 1. Transverse cut of the computational domain.

showed that rotating the cylinder breaks the symmetry of both flame branches. Since the asymmetry of both flame branches is tunable by the rotation rate, it is a variable parameter to adapt the flame topology, without changing the flow velocity or the cold gas mixture. The dynamic response of both flame branches and their interaction nevertheless remain unknown.

This article focuses on influence of the cylinder rotation rate on the dynamic response of the flames to harmonic acoustic forcing. In Section 2 the setup and numerical strategy are laid out. Section 3.1 describes the influence of the rotation rate on the unperturbed flame topology and Section 3.2 discusses the FTF of the case without cylinder rotation. This FTF is compared in Section 3.3 to FTFs for various cylinder rotation rates. Section 3.4 discusses the flame branches topology in case of monochromatic forcing for several rotation rates. Finally, the results are concluded and discussed in Section 4.

2. Configuration and simulation framework

The configuration corresponds to that of Xavier et al. [5,7]: it consists of a constant-section rectangular channel (width $W = 34$ mm and depth 94 mm) at the center of which a stainless-steel cylinder (diameter $d = 8$ mm) serves as a flame holder (see Fig. 1). The cylinder is mounted on an electric motor with a controlled rotation speed ranging from 600 to 20,000 rpm. The normalised rotation rate is defined as

$$\alpha = \frac{\omega d}{2u_b} \quad (1)$$

where u_b is the bulk velocity of the premixed gases in the channel.

As shown in previous studies on this experiment [3,5,7], because of its geometry and the laminar conditions, two-dimensional simulations are adequate. Laminar DNS are performed using the AVBP code [8], jointly developed by CERFACS and IFP Energies nouvelles, which solves the compressible Navier–Stokes equations for multicomponent reacting flows on unstructured grids. The numerical integration is performed by a two-step Taylor–Galerkin scheme called TTGC [9], which is of third-order in both space and time. In the current work, the combustion of methane and air is modelled via an analytically reduced skeletal

mechanism accounting for 19 transported species and 11 quasi-steady species [10]. This mechanism, referred to as *LU19*, is based on the *GRI-mech3.0* mechanism [11] and reproduces the adiabatic temperature and flame speed over a wide range of operating conditions. It also includes low-temperature-chemistry, required to describe flame wall interaction at the flame holder interface.

The lateral walls are water-cooled and modelled by a no-slip iso-thermal boundary condition ($T_{\text{wall}} = 292$ K). The computational domain extends from $x = -35$ mm to $x = 97$ mm, where $x = 0$ corresponds to the center of the cylinder. The inlet and outlet boundary conditions are modelled via the Navier–Stokes characteristic boundary conditions (NSCBC) [12]. The inlet is fed by a methane-air mixture at equivalence ratio $\Phi = 0.75$ and temperature $T_u = 292$ K. The velocity profile is given by experimental measurements. The bulk speed is $u_b = 0.8$ m/s. A pressure of $p = 100,700$ Pa is imposed at the outlet. This operating point is far away from flame detachment of the cylinder.

The boundary condition at the cylinder's surface is a no-slip rotating wall, which was shown by Mejia et al. [7] to accurately account for the rotation of the flame holder. An estimation of the Biot number of the present cylinder is 0.01, meaning that the assumption of spatially uniform temperature is valid. Consequently, the cylinder temperature, T_{cyl} , can be obtained by solving [5]:

$$\frac{dT_{\text{cyl}}}{dt} = \frac{S}{C_p \rho V} (\dot{Q}_{\text{cond}} - \dot{Q}_{\text{rad}}), \quad (2)$$

where t denotes time, S the cylinder surface, ρ and V the density and the volume of the cylinder, and C_p the mass specific heat capacity. \dot{Q}_{cond} and \dot{Q}_{rad} are the conductive and radiative heat fluxes, respectively. \dot{Q}_{cond} is obtained by integrating the laminar DNS heat flux long the cylinder surface. Radiation is governed by the Stefan–Boltzmann-radiation law [13]:

$$\dot{Q}_{\text{rad}} = \epsilon \sigma (T_{\text{cyl}}^4 - T_{\text{wall}}^4), \quad (3)$$

where σ is the Stefan–Boltzmann constant, and the emissivity coefficient, ϵ , is set to 0.9. The gas is assumed to be fully transparent and the temperature of the surroundings of the cylinder is supposed to be equal to the temperature of the cooled walls $T_{\text{wall}} = 292$ K. Since the time scales of the chemical reactions and that of the preheating of the cylinder are distinctively different, the transient heat up of the experiment can be accelerated following, for example the strategy presented in [14]. Also, because of the low Biot number and the high rotation rate, once in the permanent regime, the temperature of the cylinder is homogeneous and constant.

Finally, regarding spatial resolution, the coarsest cell size in the domain is $\Delta x = 500$ μm , while it is $\Delta x = 70$ μm close to the flame, which corresponds to 8 points in the flame [15]. Based on a

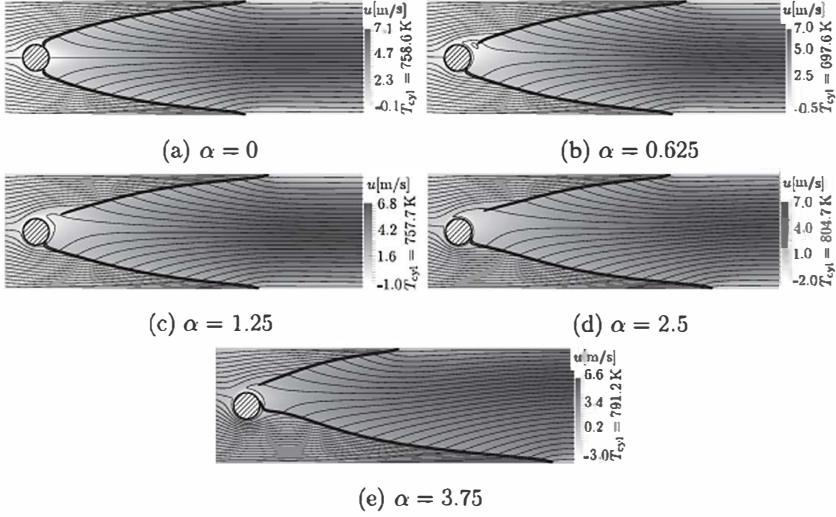


Fig. 2. Field of velocity component in main flow direction, u , with stream lines highlighted as thin black solid lines, iso-surface of heat release as thick solid line and cylinder temperature for various cylinder rotation rates, α .

mesh convergence study focusing on one dimensional flame head on quenching, the cell size at all solid walls is set to $\Delta x = 25 \mu\text{m}$. The setup of the mesh convergence study is presented in [16].

This numerical strategy was successfully compared to experimental results in many previous studies [3,5,7], including investigations on flame wall interaction [16] and it is used here without modification.

3. Results

In this section, the influence of rotation of the flame holder on the response of the flame to acoustic waves is studied. This analysis is conducted in the framework of FTF, i.e., in the linear regime corresponding to low amplitude perturbations.

3.1. Steady-state analysis

First, the steady flame shapes are presented in Fig. 2, for all of which the fluctuations in heat release are smaller than 0.05% of the mean heat release value. As expected, without rotation the flame is symmetric (Fig. 2a) but this symmetry is broken by the rotation of the flame holder. With increasing rotation rates, the root of the upper branch detaches from the cylinder, but moves upstream again for very large values of α (cf. Fig. 2e). The tip of the upper branch moves downstream until $\alpha = 1.25$ but then goes back upstream, even past its location for the symmetric flame. Regarding the lower branch, it always remains attached to the cylinder and its tip is monotonously pushed downstream. A thorough investigation of the effect of bluff body

rotation on the flame root is provided by Xavier et al. [5].

From the simple observation of the flame shape in the steady state, one can anticipate that the two branches will have a very different response to acoustic waves. Indeed, one can show from first principles [17,18] that the flame response is driven by its length and the dynamics of its root. While the length greatly impacts the delay, the dynamics of the flame root drives the gain of the FTF [4,6]. Moreover, the rotation of the cylinder breaks the symmetry of the flow so that the bulk velocities on both sides of the flame holder are different. This will change the speed at which perturbations travel on the flame front, also impacting the flame delay. Finally, because of the complex flow pattern around the cylinder, the temperature of the flame holder changes with the rotation rate (see right side of Fig. 2). It first decreases significantly at low rotation rates and increases again, past the reference value without rotation. The quantitative measurement of these changes is reported in Table 1, which gives the cylinder temperature, the flame root and tip positions and the bulk velocities for the two branches for various rotation rates.

All these changes in the flame front topology and the flow field point towards a modification of the FTF, which will be studied in the next sections.

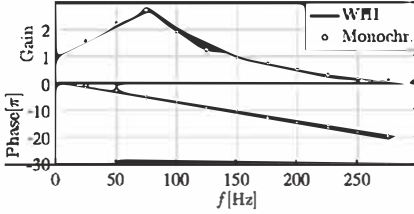
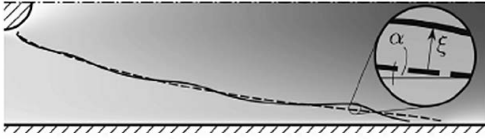
3.2. Flame response without rotation

This section focuses on the FTF of the various flames, starting with the case without rotation. Under the assumption that the system is linear and invariant, it has been shown in many studies that the Wiener–Hopf Inversion (WHI) is a pow-

Table 1

Properties taken from the laminar DNS solution for different rotation rates, α .

α	T_{cyl} (K)	x_{root,y^-} (mm)	x_{root,y^+} (mm)	x_{tip,y^-} (mm)	x_{tip,y^+} (mm)	v_{y^-} (m/s)	v_{y^+} (m/s)
0	758.6	1.9	1.9	60.1	60.1	1.05	1.05
0.625	697.6	2.4	7.8	63.4	67.3	1.08	1.02
1.25	757.7	2.4	12.1	65.2	68.2	1.12	0.97
2.5	804.7	3.4	14.8	74.8	62.2	1.26	0.83
3.75	791.2	4.3	8.3	90.1	44.5	1.46	0.64

Fig. 3. FTF without rotation ($\alpha = 0$) based on WHI and monochromatic forcing.Fig. 4. Flame shapes behind a non-rotating cylinder; dashed line: unperturbed flame; solid line: flame forced at 80 Hz; Insert: definition of flame angle, α , and flame normal displacement, ξ .

erful methodology for the determination of FTFs [19–21]. In this method, the transfer function of a system is estimated by broad band forcing of the system and subsequent correlation analysis of its input and output signal. A detailed description of the method is provided in [22,23]. In order to remain in the linear regime, the forcing amplitude for the estimation of the FTF is kept at 1% of the bulk velocity. The reference point for the velocity perturbations is at $x = -10$ mm and $y = 0$. Figure 3 shows the FTF of the symmetric reference flame (i.e., $\alpha = 0$), obtained by a WHI analysis of laminar DNS data. As seen in previous studies of this configuration, this flame only responds under 250 Hz and shows a strong gain (> 2) at low frequencies, here around 80 Hz. The phase of the FTF is linear, corresponding to a constant time delay τ defined as the slope of the phase. For the present operating point, $\tau = 35.5$ ms. The accuracy of the WHI was tested by performing FTF evaluation at various discrete frequencies (see circles in Fig. 3).

We now investigate the motion of the flame front under harmonic forcing at 80 Hz, i.e., close to the frequency of the peak in the FTF. Figure 4 presents the mean and perturbed flame front and

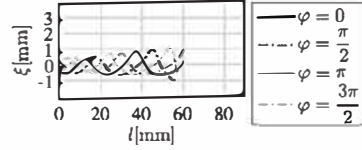
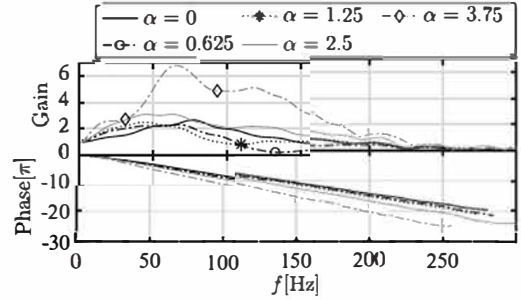
Fig. 5. Flame displacement, ξ , along the flame front without rotation for various phases at $f = 80$ Hz. Forcing amplitude: $5\%u_b$.

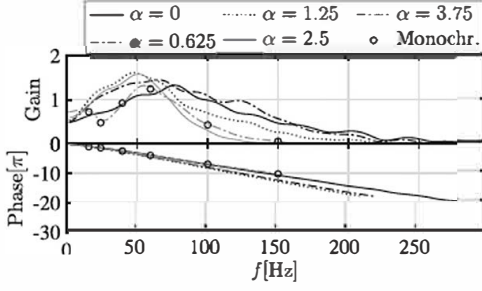
Fig. 6. Influence of flame holder rotation on the FTF.

shows the definition of the normal displacement ξ between the two. In order to elucidate the dynamics of the flame, the evolution of ξ along the flame front is presented in Fig. 5 at four different phases of the harmonic excitation. It appears that the amplitude of the displacement increases weakly along the flame front but shows non-linear deformation close to the flame tip. It is also quite clear that a lot of the variation in the flame surface is caused by the flame-wall interaction at the flame tip.

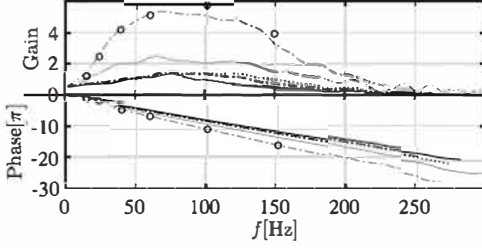
3.3. Flame response with rotation

Figure 6 shows the FTFs for various rotation rates, up to $\alpha = 3.75$, including the case without rotation as the reference. The first observation is that the maximum gain is marginally affected up to $\alpha = 2.5$. However, between $\alpha = 2.5$ and $\alpha = 3.75$, it increases by at least a factor of 2. The location of the maximum gain remains in the low-frequency range (between 50 Hz and 80 Hz), but without clear trend.

The second observation is that for many rotation rates, the gains exhibit strong dips (see markers



(a) Upper flame branch (y^+).



(b) Lower flame branch (y^-).

Fig. 7. FTF of individual flame branches versus rotation rate α ; the circles mark results of monochromatic forcing at $\alpha = 3.75$.

in Fig. 6). It is anticipated that these dips could stem from the symmetry breaking of the flame, resulting in interference between the responses of the two flame branches. Regarding the phase of the FTF, it is linear in all cases and the corresponding delay monotonously increases with the rotation rate.

In order to investigate the dips in the FTF gain, the two flame branches are now analysed separately. The underlying assumption is that their dynamics are not, or sufficiently weakly coupled.

The FTF of the upper ($y > 0$, labelled y^+), respectively lower ($y < 0$, labelled y^-) branches are determined by integration of the heat release rate over one half of the domain. The reference point for the velocity is the same as for the global FTF and the heat release rate fluctuations are normalised by the total flame power. The resulting FTFs are displayed in Fig. 7a for the y^+ -branch and in Fig. 7b for the y^- -branch.

For the upper branch, the variations in maximum gain are limited but the cutoff frequency clearly decreases with α . It goes from 250 Hz without rotation down to around 130 Hz for $\alpha > 2.5$. The delay of the flame response first increases and then decreases with a maximum around $\alpha = 1.25$, which is consistent with the evolution of the steady upper-flame length shown in Fig. 2.

The evolution of the FTF of the lower branch is very different. First there is no decrease in the cutoff frequency but the striking feature is that the maximum gain increases drastically past $\alpha = 2.5$

over a broad frequency range. The delay of the FTF monotonously increases with α , replicating the increase in flame length concomitant with the bulk velocity increase for $y < 0$. Despite the high gains at $\alpha = 3.75$, results of monochromatic forcing, which are illustrated by the circles in Fig. 7, and WHI are in good agreement.

We now investigate the hypothesis that the breaking of the flame symmetry results in an interference between the two branches. A practical application for this modification of the FTF via rotation of the flame holder could be the control of combustion instabilities by tuning the location of the dips in the FTF. A simple model can be built to predict the frequency at which this dip occurs. It is based on the idea that the dip is the consequence of the interference between the responses in heat release fluctuation of the two branches. The total heat release fluctuation is equal to the sum of the heat release fluctuation of both branches, $q'_{\text{tot}} = q'_{y^+} + q'_{y^-}$. Introducing the FTF using the notation of Crocco, the fluctuation in heat release can be related to a harmonic velocity fluctuation, u' , which yields:

$$\frac{q'_{\text{tot}}}{\bar{q}} = \frac{u'}{\bar{u}} (n_{y^+} + n_{y^-} \exp(i\omega\Delta\tau)) \exp(i\omega\tau_{y^+}). \quad (4)$$

Here, n are the gains of the respective branches and the difference in time delays is depicted as $\Delta\tau = \tau_{y^-} - \tau_{y^+}$. From Eq. (4) it is evident, that the gain of the global FTF is depending on the phase angle between the two branches, given by

$$\Delta\phi = \omega\Delta\tau. \quad (5)$$

The two extreme cases are ideal constructive interference and ideal destructive interference. For the former case, the phase angle between the both branches' heat release signals is 0 or an even multiple of π . Then the gain of the global heat release reduces to $n_{\text{tot}} = n_{y^+} + n_{y^-}$. In the other case, the difference in phase angles is an odd multiple of π , so that the gain of the global heat release is equal to $n_{\text{tot}} = |n_{y^+} - n_{y^-}|$. Therefore, the frequency at which destructive interference is maximal can be deduced from Eq. (5):

$$f_{d,n} = \frac{\Delta\phi}{2\pi\Delta\tau}, \quad \Delta\phi = (2n - 1)\pi, \quad n \in \mathbb{Z}. \quad (6)$$

The values, extracted from the laminar DNS, of the delays of the two branches (τ_{y^+} and τ_{y^-} for the upper and lower branch, respectively), their difference, $\Delta\tau$, and the first two frequencies of constructive and destructive interference ($f_{c,n}$ and $f_{d,n}$ for $n = 1$ and $n = 2$) are given in Table 2. For $\alpha = 0.625$ and $\alpha = 1.25$, the predicted values of $f_{d,1}$ correspond very well to the FTF of Fig. 6. For $\alpha = 2.5$, the first destructive interference occurs at a frequency where the gain of the upper-branch FTF is close to zero (cf. Fig. 7a). Consequently, the interference is not meaningful and no dip is observed in the FTF. Finally for the higher rotation rate ($\alpha =$

Table 2

Time delays of the two flame branches ($\tau_{y,+}$ and $\tau_{y,-}$ for the upper and lower branch, respectively) and values of the first two frequencies for destructive and constructive interference (cf. Eq. (6)).

α	$\tau_{y,+}$ (ms)	$\tau_{y,-}$ (ms)	$\Delta\tau$ (ms)	$f_{d,1}$ (Hz)	$f_{d,2}$ (Hz)	$f_{e,1}$ (Hz)	$f_{e,2}$ (Hz)
0.0	35.5	35.5	0	—	—	—	—
0.625	40.9	37.1	-3.8	132	395	263	395
1.25	42.5	37.9	-4.6	109	326	217	435
2.5	38.6	41.6	3.0	167	500	333	667
3.75	33.6	49.7	16.1	31	93	62	124

3.75), the value of $f_{d,1}$ is again very low and a dip is observed.

The frequency of the second dip, $f_{d,2}$, (Table 2) is much higher than the cutoff frequency of the flame response for all rotation rates except for $\alpha = 3.75$, which exhibits a dip around the expected value of 93 Hz. The frequencies $f_{d,n}$ are illustrated by the markers in Fig. 6, showing very good agreement with the location of the dips in the corresponding gains. It seems that the simple model of Eq. (6) gives an accurate prediction of this phenomenon, giving a posteriori confirmation of the hypothesis that there is indeed interference between the two flame branches.

Given the strong impact of symmetry breaking on the shape of the FTF, one may use the rotation rate of the flame holder to control combustion instabilities. However, it can be anticipated that only the low rotation rates, say $\alpha < 1.25$ can be of practical use for the present flame, first because of the strong decrease of the cutoff frequency of one of the branches, but also because of the large increase in gain of the other branch, which drives the gain of the total FTF and hinders the destructive interference.

3.4. Flame front dynamics

We pursue the analysis of the flame response by plotting the flame displacement along the flame front for the two branches in Fig. 8. As for the non-rotating case, the frequency of interest is 80 Hz, which lies close to the peak in the gain of the FTF for all rotation rates.

We start the analysis for the upper flame branch. For all rotation rates a growth of the flame displacement along the flame front is observed. With increasing rotation rate from $\alpha = 0$ to $\alpha = 2.5$, the flame displacement amplitude at the flame tip decreases moderately. It appears that the response in flame displacement amplitude increases again beyond this rotation rate. The same trend can be observed regarding the non-linear deformation close to the flame tip. This effect seems to decrease until a rotation rate of $\alpha = 2.5$ and increase again for higher rotation rates. Nevertheless, only a small variation of the flame displacement amplitude at the flame tip is observed. At the lower flame branch,

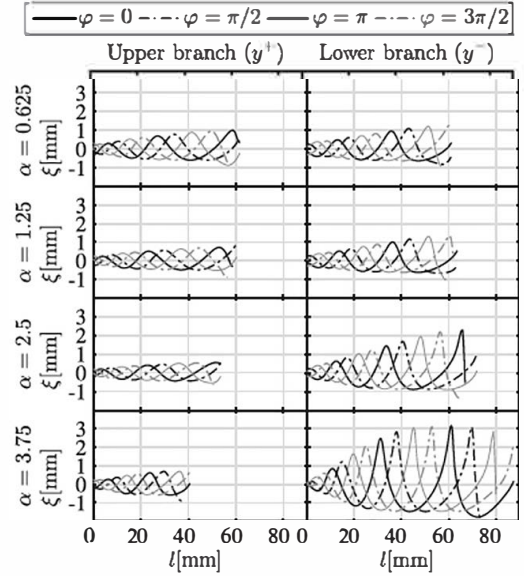


Fig. 8. Flame displacement, ξ , along the flame front at a velocity forcing of amplitude of $5\% u_b$ and $f = 80$ Hz for various phase angles, φ , and rotation rates α .

the amplitude of the flame root displacement at $l = 0$ seems to decrease with increasing rotation rate. In contrast, the displacement growth along the flame front significantly increases, especially for rotation rates of $\alpha \geq 2.5$. This goes along with a considerable increase in non-linearity, as can be seen in the right half of Fig. 8. Note that the flame displacement monotonically grows along the flame front for both the upper and the lower branch and all rotation rates until the flame tip, except for the lower branch at $\alpha = 3.75$. Here a saturation seems to occur and the fluctuation amplitude, while initially growing at the highest rate for low flame locations, stays approximately constant for $l > 40$ mm until the flame tip at $l = 87.4$ mm. Figure 8 suggests, that the lower branch's drastic increase in gain of the FTF for rotation rates $\alpha \geq 2.5$ might be due to some kind of convective instability mechanism which leads to a significant increase in flame displacement. The growth of perturbations artificially introduced into

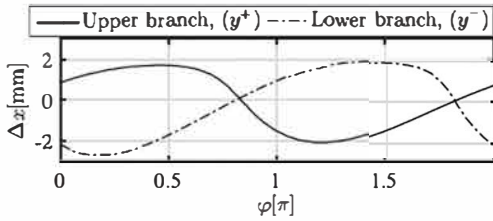


Fig. 9. Relative flame tip position with respect to the flame tip position of the steady flame, $\Delta x = x_{tip} - x_{tip,s}$, as a function of the phase angle of the velocity perturbation, φ , for a cylinder rotation rate of $\alpha = 0.625$; pulsation amplitude: 2% of bulk velocity; pulsation frequency: 132 Hz.

a laminar flame has been observed before (e.g., by Petersen [24] and Mejia et al. [4]).

Finally, the flame tip movement is analysed. Figure 9 shows the flame tip position of the perturbed upper and lower flame branches with respect to their positions in the unperturbed case for a cylinder rotation rate of $\alpha = 0.625$. The pulsation amplitude is at 2% of the bulk speed and its frequency is 132 Hz, i.e., at the frequency of ideal destructive interference. It appears that the tip movements are perfectly out of phase, which is expected since at these frequencies the FTFs show a phase difference of π and most of the heat release fluctuation is produced at the interaction of the flame tip and the lateral walls. Together with Fig. 6, Fig. 9 shows that introducing rotation of a flame holder can be used to build a flame which becomes almost insensitive to acoustic perturbation, suggesting that this could be used for combustion instability control. Note however that this result is obtained only in a limited frequency range.

4. Conclusion

The FTF of a laminar flame stabilised behind a rotating cylindrical bluff body is investigated for various rotation rates of the cylinder by the means of laminar DNS. The rotation causes a symmetry break between the two flame branches, where especially the flame tip positions vary significantly, especially for high rotation rates. FTFs are estimated for each branch separately, assuming that they can be described as two independent Linear Time Invariant (LTI)-systems. The results show a difference in time delays between the upper and the lower flame branch. This is mainly due to an independent modification of the flame tip positions of both branches, caused by two effects: a detachment of the upper branch from the cylinder and a modification of the bulk speeds in the two half domains due to the cylinder's viscous boundary layer. The resulting difference in time delay causes interference of the flames' heat release signals. At

frequencies where destructive interference is maximal, the global FTFs, which include both flame branches, as a consequence show deep gaps in the gain. The difference in time delay and therefore the frequency at which destructive interference of both flame branches occurs can be tuned by adapting the rotation rate of the cylinder. In this context, the analysis suggests, that the rotation rate is a suitable and easily adaptable measure of open loop control of combustion instabilities. It is shown that for cylinder rotation rates, $\alpha \geq 2.5$, the flame displacement considerably grows along the flame front of the lower flame branch, leading to gains, that by far exceed the gain of the non-rotating configuration. This effect therefore limits the applicability of the method to moderate rotation rates and frequencies $f \geq 100$ Hz. Most practical flames are highly turbulent, and the existence of a corresponding effect in the turbulent regime remains unknown. Nevertheless, the present paper underlines the asset of decreasing the gain of the FTF significantly around a specific frequency by being able to tune the asymmetry of a combustion system which leads to destructive interference.

Acknowledgments

The research leading to these results has received funding from the European Research Council under the European Union's Seventh Framework Programme (FP/2007-2013)/ERC Grant Agreement ERC-AdG 319067-INTECOCIS.

This work was granted access to the high-performance computing resources of CINES under the allocation A0032B07036 made by Grand Equipement National de Calcul Intensif.

References

- [1] R. Blumenthal, P. Subramanian, R. Sujith, W. Polifke, *Combust. Flame* 160 (2013) 1215–1224.
- [2] T. Schuller, D. Durox, S. Candel, *Combust. Flame* 134 (2003) 21–34.
- [3] M. Miguel-Brebion, D. Mejia, P. Xavier, et al., *Combust. Flame* 172 (2016) 153–161.
- [4] D. Mejia, M. Miguel-Brebion, A. Ghani, et al., *Combust. Flame* 188 (2018) 5–12.
- [5] P. Xavier, A. Ghani, D. Mejia, et al., *J. Fluid Mech.* 813 (2017) 127–151.
- [6] D. Mejia, L. Selle, R. Bazile, T. Poinsot, *Proc. Combust. Inst.* 35 (2015) 3201–3208.
- [7] D. Mejia, M. Bauerheim, P. Xavier, B. Ferret, L. Selle, T. Poinsot, *Proc. Combust. Inst.* 36 (2017) 1447–1455.
- [8] T. Poinsot, *The AVBP Handbook*, CERFACS, Toulouse, 2005.
- [9] O. Colin, M. Rudgyard, *J. Comput. Phys.* 162 (2000) 338–371.
- [10] T. Lu, C.K. Law, *Combust. Flame* 154 (2008) 761–774.

- [11] P.S. Gregory, D.M. Golden, M. Frenklach, et al., GRI-Mech, 2000. http://www.me.berkeley.edu/gri_mech/ (Accessed: 23 June 2018).
- [12] T. Poinsot, S. Lele, *J. Comput. Phys.* 101 (1992) 104–129.
- [13] L. Boltzmann, *Ann. Phys.* 258 (1884) 291–294.
- [14] F. Duchaine, A. Corpron, L. Pons, V. Moureau, F. Nicoud, T. Poinsot, *Int. J. Heat Fluid Flow* 30 (2009) 1129–1141.
- [15] M. Brebion, *Joint Numerical and Experimental Study of Thermo-acoustic Instabilities*, Institut de Mécanique des Fluides de Toulouse, 2016 Ph.D. thesis.
- [16] A. Ghani, T. Poinsot, *Flow Turbul. Combust.* 99 (2017) 173–184.
- [17] L. Boyer, J. Quinard, *Combust. Flame* 82 (1990) 51–65.
- [18] A. Cuquel, D. Durox, T. Schuller, *C. R. Méc.* 341 (2013) 171–180.
- [19] A. Giauque, T. Poinsot, F. Nicoud, 14th AIAA/CEAS Aeroacoustics Conference, Vancouver, British Columbia, Canada (2007) 2943.
- [20] A. Gentemann, C. Hirsch, K. Kunze, F. Kiesewetter, T. Sattelmayer, W. Polifke, Proceedings of ASME Turbo Expo, Vienna, Austria(2004) 501–510.
- [21] W. Polifke, A. Poncet, C. Paschereit, K. Döbbling, *J. Sound Vib.* 245 (2001) 483–510.
- [22] L. Ljung (Ed.), *System Identification (2nd ed.): Theory for the User*, Prentice Hall PTR, Upper Saddle River, NJ, USA, 1999.
- [23] A. Huber, W. Polifke, *Int. J. Spray Combust. Dyn.* 1 (2009) 199–228.
- [24] R.E. Petersen, H.W. Emmons, *Phys. Fluids* 4 (1961) 456–464.